Science of the Total Environment 770 (2021) 145490

Contents lists available at ScienceDirect

Science of the Total Environment

journal homepage: www.elsevier.com/locate/scitotenv

Impact of compost reactive layer on hydraulic transport and C & N cycles: Biogeochemical modeling of infiltration column experiments

Arnau Canelles [a,b,*], Paula Rodríguez-Escales [a,b], Jakub Jan Modrzyński [c], Christian Albers [c], Xavier Sanchez-Vila [a,b]

[a] Dept. of Civil and Environmental Engineering, Universitat Politècnica de Catalunya, Jordi Girona 1-3, 08034 Barcelona, Spain
[b] Associated Unit: Hydrogeology Group (UPC-CSIC), Spain
[c] Department of Geochemistry, Geological Survey of Denmark & Greenland (GEUS), Copenhagen, Denmark

HIGHLIGHTS

- A reactive barrier has a significant effect in nutrient and hydraulic dynamics, both long and short term.
- Compost increases biological activity and adds new processes (e.g. DNRA).
- A mixture of sand/compost behaves hydraulically as a dual porosity model, non-Fickianity increasing over time

GRAPHICAL ABSTRACT

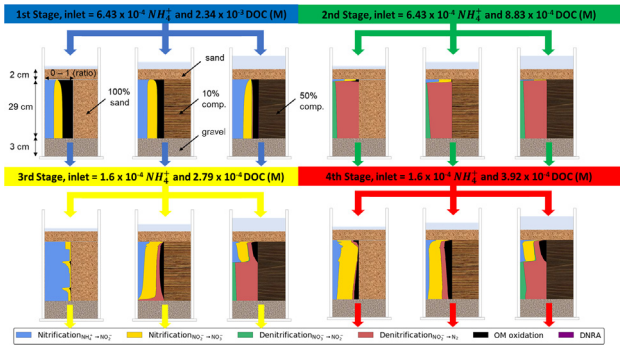

ARTICLE INFO

Article history:
Received 14 September 2020
Received in revised form 29 December 2020
Accepted 25 January 2021
Available online 30 January 2021

Editor: Christian Herrera

Keywords:
Managed aquifer recharge
Reactive transport modeling
Nitrogen cycle
Bioclogging
Column experiments

ABSTRACT

Managed Aquifer Recharge (MAR) is a key strategy to increase freshwater resources in many regions facing water scarcity. MAR issues are related to both quantity and quality of the infiltrating water. In most countries, very high quality of the infiltrating water is required, to limit the impact on the aquifer geochemistry. In this paper, the possibility of injecting water of lower quality in the aquifer and letting the biogeochemical reactions take place in order to enhance its quality is explored. Here, we present the fate of nutrients (C, N) in the biogeochemical system of a reactive barrier formed by mixture of different proportions of sand and compost, supplied with treated wastewater to mimic MAR. An integrated conceptual model involving the nutrient cycles and biomass dynamics (auto- and heterotrophic) was developed, and then tested with a number of solute transport experiments in columns with different compost fraction in the column filling. The model incorporated both saturation and inhibition processes (regarding the nutrients and their byproducts) to provide a comprehensive picture of the nutrient dynamics within the column. The model developed (three if considering the 3 column setups) allowed to discriminate the processes that govern the fate of nutrients in relation with the compost enhancing long-term nutrient degradation, yet hindering hydraulic parameters that affect infiltration rates.

1. Introduction

Managed aquifer recharge (MAR) is a well-established technology capable of increasing the water resources storage with the purpose of either later being recovered for different uses (agricultural, industrial or urban). It can also be used for obtaining environmental benefits,

* Corresponding author at: Dept. of Civil and Environmental Engineering, Universitat Politècnica de Catalunya, Jordi Girona 1-3, 08034 Barcelona, Spain.
E-mail address: arnau.canelles@upc.edu (A. Canelles).

https://doi.org/10.1016/j.scitotenv.2021.145490
0048-9697/

such as: reducing the physical impacts in rivers and lakes (mainly geological natural formations) due to water storage structures (dams mainly) for drinking purposes; reducing saline intrusion due to well over-exploitation; protection of local wildlife due to ecosystem preservation (without the anthropic modification of lakes and rivers, wildlife can maintain their original ecosystems), among other (Dillon et al., 2019). Consequently, MAR emerges as an efficient tool to minimize water scarcity, especially in arid and semi-arid regions, such as the Mediterranean basin (Rodríguez-Escales et al., 2018). Water scarcity, to be exacerbated in the future due to climate change, combined with high population density, draw an alarming scenario for water security in the Mediterranean region and worldwide in the coming decades (IPCC, 2007; Giorgi and Lionello, 2007; Pedretti et al., 2012).

The two main controversial topics that are limiting the widespread implementation of MAR facilities are the infiltration rate capacity losses over time and the quality of the infiltrating water (e.g. Rodríguez-Escales et al., 2018). The infiltration rate capacity decreases with time driven by the physical and chemical characteristics of the water supplied to the MAR facility and to the actual technology used for recharge (Dillon et al., 2019). Physical and biological clogging are two main reasons of infiltration rate loss (Carles Brangarí et al., 2017; Rodríguez-Escales et al., 2018). Whereas physical clogging depends on the size and amount of particles in suspension in the input water (Pedretti et al., 2012), bioclogging is mostly controlled by biofilm growth on soil grains that conform the porous media, reducing the effective size of the pores. Biofilm growth is mainly governed by the concentration of supplied nutrients and by temperature.

The quality of the infiltrating water mainly depends on the biochemical signature of the input water and the reactions that take place within the system (mainly the top few cm). Due to the combination of environmental and human health protection laws, in some cases the biogeochemical signature of the water that can legally be infiltrated are restrictive, in some cases allowing only the infiltration of water of drinking quality (Dillon et al., 2019) or even osmotized water (Ganot et al., 2018). On the contrary, two most common sources of water supplied to MAR facilities are excess river water in flood episodes, and effluents from wastewater treatment plants (WWTPs, after either secondary or tertiary treatment). In the latter case, MAR actions can be considered as a solution to re-naturalize wastewater, within the context of circular economy (Dillon et al., 2010), where treated wastewater should be seen as a resource rather than a waste (Van Der Hoek et al., 2016).

However, due to the abovementioned concerns about water quality, the usage of wastewater outflow has been limited and dependent on the type of MAR technology (Maliva and Missimer, 2012). Nevertheless, we contend that using water with drinking standard quality for aquifer recharge is a very narrow vision, as looking exclusively to the quality of the supplied water overlooks and ignores the purifying capacity of the subsoil, which can considerably improve water quality (Silver et al., 2018). Rather, we focused in the quality of water once it reaches the aquifer, or even the discharge point, being either a well, a spring or a body of surface water. Consequently, MAR facilities implementation must track the evolution of water quality along the infiltration path and with time. This implies tracking the fate of different target compounds, and, to enhance attenuation processes during recharge within the context of soil-aquifer remediation technologies. In the case of nitrogen compounds present in the recharged water (NH_4^+, NO_3^-, NO_2^-), limitations in the accepted concentrations for water to be used in MAR facilities is linked to the risk for humans to develop methahemoglobine or stomach cancer, or else to promote water eutrophication (Grau-Martínez et al., 2018, 2017; Maeng et al., 2011; Miller et al., 2006). Therefore, the goal would be to create an environment capable of completely reducing the N-compounds and promoting the formation of dinitrogen gas, being a harmless compound. That means promoting a reductive environment, which normally is conditioned by the presence of labile organic carbon (OC, acting as an electron donor in a reduction-oxidation system). Since the concentration of labile OC in the aquifer is low, a potential solution to enhance the metabolism of nitrogen compounds is the addition of an external pool into the system. In the context of a MAR facility involving an infiltration pond, this can be achieved by the installation of a reactive layer partially composed of organic carbon into the bottom of a pond (Alazard et al., 2016; Dillon et al., 2009; NRMMC, 2006; Valhondo et al., 2014).

A successful experience in this regard was the installation of a permeable reactive layer at the MAR system placed at the Llobregat Lower Valley (Valhondo et al., 2014) near Barcelona (Spain); this layer enhanced not only the degradation of nutrients and emerging organic compounds, but also the biological activity of the subsoil (Barba et al., 2019). Different materials for organic layers have been tested and reported in the literature, several of them sharing similar concentration values in labile organic carbon. For example, organic substrates such as compost (Grau-Martínez et al., 2017; Schaffer et al., 2015; Valhondo et al., 2014), softwood (Gibert et al., 2008) and palm leaves (Grau-Martínez et al., 2017) were tested with positive results in terms of the reduction of nitrogen compounds in experiments under batch conditions.

The Nitrogen cycle is complex, as processes depend on the redox state of the system and the presence of biomass (quantity, diversity, density, etc.). The most common nitrogen-compound present in a WWTP outflow is ammonium, NH_4^+, which can be oxidized to nitrate, NO_3^-, in the presence of oxygen, catalysed by autotrophic biomass (nitrification). Nitrate can then be reduced to dinitrogen gas, N_2, in the presence of an electron donor by either autotrophic or heterotrophic biomass (denitrification). Both nitrification and denitrification processes are sequential, forming a suite of intermediate nitrogen compounds (e.g., NO_2^-, NO, or N_2O). Their formation should be avoided; first, NO_2^-, is quite a harmful compound that can be accumulated during either nitrification or denitrification; second, NO_x are greenhouse gases. Finally, the processes of dissimilatory nitrogen reduction to ammonia (DNRA), using organic carbon as electron donor and potentially accumulating nitrite (Grau-Martínez et al., 2017; van den Berg et al., 2016), is quite common in the nitrogen dynamics, thus introducing more complexity to the system.

In this way, it is quite important to improve the knowledge about the impact of a reactive barrier in the processes governing the fate of nitrogen compounds, especially concerning the accumulation of hazardous products (ammonia, nitrite or NO_x). Geochemical modeling is particularly useful to improve this understanding. In the literature, there are different conceptual models for the N-cycle in the subsoil, incorporating only a subset of the processes described, such as nitrification (Koper et al., 2010; Urakawa et al., 2016), denitrification (Green et al., 2008; Mastrocicco et al., 2011; Rodríguez-Escales et al., 2016) or DNRA (Rubol et al., 2013). Nevertheless, most of them do not include the interrelation between processes and reactions (Schmidt et al., 2012), or do not account for changes in input dynamics that define the evolution of the biological community in the system (Akhavan et al., 2013).

Besides, the enhancement of degradation enforced by the presence of a reactive layer would imply an increase in biomass production, and, consequently, a significant biofilm growth leading to partial pore network clogging. In this way, the evaluation of the risk of clogging as a function of time and distributed in space due to the installation of an organic reactive layer is not yet available in the literature.

Considering all of these, the main aim of this work is to develop a comprehensive geochemical model of carbon and nitrogen dynamics in porous media, aimed at determining the impact of a reactive layer in the context of managed aquifer recharge. As a side objective, we want also to evaluate changes in transport parameters due to biofilm growth induced by the presence of such reactive layer. To this end, we present the conceptual model describing interrelation between biogeochemistry and hydraulic parameters. Subsequently, the model is validated with data from a set of column experiments (Modrzyński, 2021) developed with different proportions of compost (being the source of labile organic carbon) and sand. Finally, we present the results of the model allowing for a thorough discussion of biogeochemical and hydraulic processes and calibrated parameters.

2. Methodology

In this work, three sequential steps were considered: (1) conservative transport analysis and modeling, setting the baseline for the evaluation of the potential effect of biofilm growth upon transport; (2) building the conceptual model for the biologically catalysed geochemical reactions; and (3) construction of the numerical model and its implementation. Finally, the numerical model is verified with flow through experimental data in columns from (Modrzyński, 2021).

2.1. Flow and conservative transport model: evaluation of the impact of biofilm growth upon transport parameters

The first step was to create the flow and the conservative transport models. We assumed transport in bioclogged porous media to be well described by a dual porosity model (e.g., Haggerty and Gorelick, 1995; Lawrence et al., 2002), already used frequently in the literature to model a number of tracer tests in column experiments (Delay et al., 2013; Rodríguez-Escales and Sanchez-Vila, 2016; Seifert and Engesgaard, 2007). A dual porosity domain model represents the porous medium as composed of a mobile and one (or alternatively a suite of) immobile fluid porosity regions that coexist. In the former, representing the volume occupied by the aqueous phase, advection and dispersion are the main driving processes; in the latter, being the region where biofilm dynamics derived from the growth of heterotrophic and autotrophic biomass take place attached to the sediment, only diffusion is considered. Both regions exchange mass proportionally to the difference in their concentrations at any given time. The equation describing the concentration of species *i* in the mobile zone, $c_{m,i}$, here assuming a simple one-dimensional domain as it will be later applied to column experiments, is:

$$\phi_m \frac{\partial C_{m,i}}{\partial t} = -q\frac{\partial C_{m,i}}{\partial x} + \phi_m D\frac{\partial^2 C_{m,i}}{\partial x^2} - \Gamma_i \quad (1)$$

where D is the dispersion coefficient, q is specific discharge, ϕ_m the porosity corresponding to the mobile zone, and Γ_i the source-sink term controlling the mass transfer of species *i*, between the mobile (m) and the immobile regions (im), given by:

$$\Gamma_i = \alpha\phi_{im}(C_{m,i} - C_{im,i}) \quad (2)$$

with α the mass transfer rate coefficient [T^{-1}], ϕ_{im} [−] the porosity corresponding to the immobile region (volume fraction occupied by the biofilm), and $C_{im,i}$ the concentration of species *i* in the immobile region. The actual total porosity is then $\phi_t = \phi_m + \phi_{im}$. The reason behind this porosity change is that the formation of biofilm colonizes pores that were initially occupied by water in sediments (bioclogging), so that the pores occupy the same volume at the beginning and end of the experiment. Therefore, a key parameter in characterizing the shape of the breakthrough curve in the dual porosity model is the ratio of porosities (Fernàndez-Garcia and Sanchez-Vila, 2015) given by $\beta = \phi_{im}/\phi_m$. In the limiting case of $\beta = 0$, equivalent to $\Gamma_i = 0$, Eq. (1) converges to the classical advection-dispersion equation (ADE).

2.2. Reactive transport model: processes and governing equations

2.2.1. Biogeochemical processes: nitrogen and carbon cycle

The biogeochemical conceptual model for the nitrogen and the carbon biochemical cycles is depicted in Fig. 1, showing the main processes involved. Under aerobic conditions, two processes are considered: oxidation of organic matter (process 1 in Fig. 1) and oxidation of ammonia (process 2.1 and 2.2). The former is triggered by heterotrophic biomass (indicated by 6.3 in the figure), and the latter by autotrophic one (5.1 and 5.2 in the Figure). In both cases, we considered a growth of biomass which could eventually decay and form inorganic carbon. In the case of nitrification, the oxidation of ammonia to nitrate (nitritation, process 2.1) leaves nitrite as an intermediate product which is then transformed into nitrate (nitratation, process 2.2). We did not distinguish between microbial populations (only distinguished between aerobic and anaerobic) in order to simplify the model.

Concerning anaerobic conditions, we considered oxidation of organic carbon due to denitrification, i.e., the reduction of nitrate to dinitrogen gas (process 3.1 and 3.2). This process is mainly driven by heterotrophic denitrifying biomass (6.1 and 6.2). In this case, we also considered two steps in the reduction of nitrate, as well as the transient accumulation of nitrite. The accumulation of other intermediate nitrogen compounds, *NO* and N_2O, was neglected. Besides, we also considered Dissimilatory Nitrate Reduction (DNRA, process 4), a process that implies a consumption of nitrate and organic carbon in order to generate ammonia by DNRA-specific biomass (heterotroph, number 6.4 in the Figure).

The model also describes the release of labile dissolved organic carbon (DOC) and ammonia from compost, a process independent from Eh conditions (process 7). Organic matter was considered in two fractions, easily degradable and recalcitrant, and it was considered that only the former could be degraded and therefore the latter was unaccounted for in the biogeochemical reactions.

2.2.2. Geochemical models: processes and reaction rates

The next step was the construction of the geochemical numerical model. Table 1 compiles all the reactions considered in the modeling process and sketched in Fig. 1, including the stoichiometric coefficients and the expressions for the individual reaction rates. As a general rule, we included double Monod Kinetic terms in the main redox reactions: oxidation of organic matter, nitrification, denitrification and DNRA. Reactions were assumed kinetically controlled, characterized by a set of parameters: $K_{max,\,j}$ [T^{-1}] being the consumption rates of electron donor per unit value of biomass of the "j" process; $K_{s,\,i}$ [ML^{-3}] the saturation constants of the "i" compounds; *b* [T^{-1}] a decay constant for autotrophic biomass (b_{aut}) and heterotrophic biomass (b_{het}); and $K_{I,\,j}$, [ML^{-3}] the inhibition constants for the "j" compounds. Both autotrophic and heterotrophic biomass were introduced into the model as two different immobile species; they were conceptualized as having an average chemical composition of $C_5H_7O_2N$ (Porges et al., 1956). We did not distinguish between different autotrophic biomass, e.g. ammonia-oxidizing bacteria or nitrite-oxidizing bacteria since it would increase complexity and uncertainty in the model. Nevertheless, we distinguish between total heterotrophic biomass and denitrifying and DNRA biomass by adding a ratio into the model ($\alpha_1 = 0.1$ and $\alpha_2 = 0.05$, respectively). The release of organic carbon from compost was modeled as first order kinetics. Here, compost was defined as an immobile species, with a stoichiometric of compost release calibrated to fit the experimental data of organic matter and ammonia.

2.3. Description of the experiment and data set

The conceptual model described was then applied to interpret a number of column experiments available in the literature (Modrzyński, 2021), aiming at finding the impact of the addition of different proportions of compost within soil material (sand) in the different compounds involved in the nitrogen cycle. These infiltration experiments consisted of five treatments with two replicates each (a total of 10 columns) that ran for a total time of 116 days. The water flow in the column was vertical (top to bottom) fixed at 0.5 ml/min. The columns were 6.6 cm of interior diameter, and composed of a top layer of field sand (2–2.5 cm) underlain by the 29 cm-long reactive layer (for the different proportions of field sand and vegetal compost, see Table 2), with a coarse silica sand layer at the bottom (3 cm). For the compost molar composition, we considered a chemical formula of $C_{204}\,H_{325}\,O_{85}\,N_{77}\,S$, and an average density of 550 Kg/m^3. For further details on the column setup and

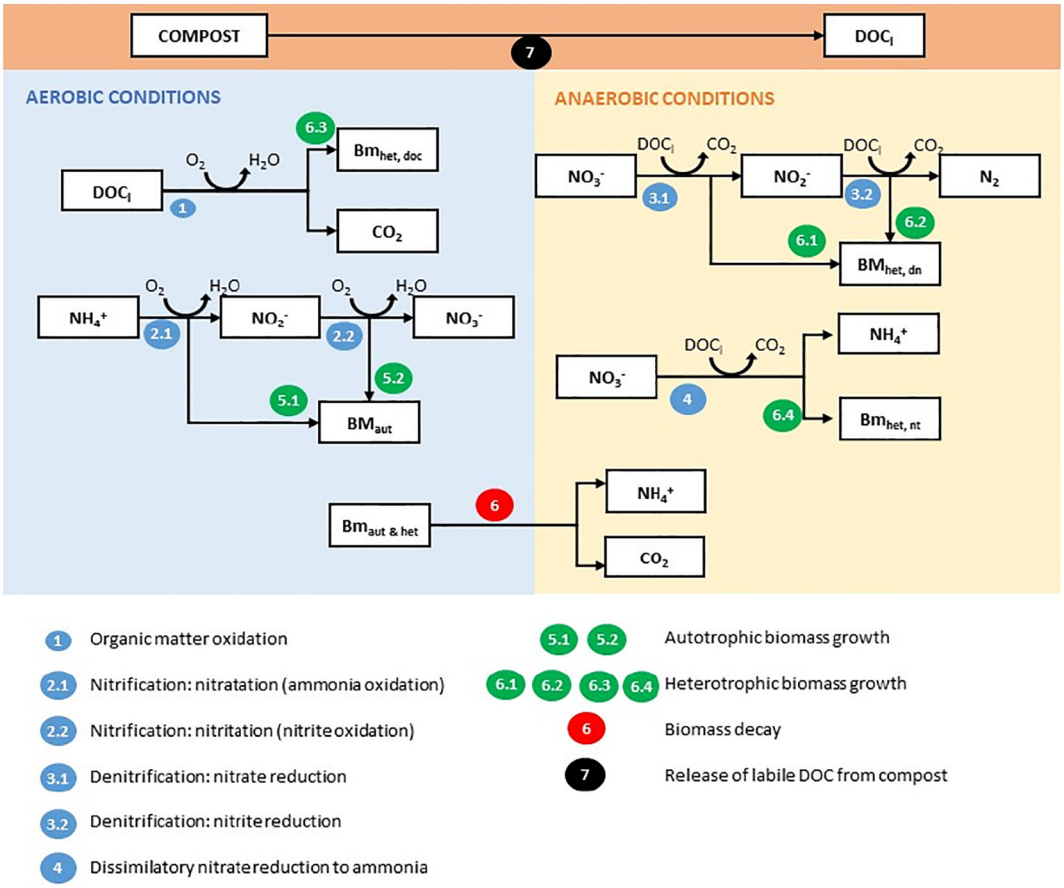

Fig. 1. Conceptual model of biogeochemical processes occurring during column experiments. In aerobic conditions, the reactions included are nitrification (two steps, from ammonium to nitrite and then to nitrate) and labile organic matter oxidation. For the anaerobic reactions, denitrification (two steps, from nitrate to nitrite and then to nitrogen gas) and DNRA (which implies the conversion of nitrate into ammonium). Finally, the biomass (auto and hetero) decay is included (which generates carbon dioxide and ammonium).

reactive barrier composition, see Modrzyński, 2021 and Valhondo et al., 2020. In addition, selected columns were inoculated with real wastewater (activated sludge) for a short period of time (see Table 2), in order to test the effect of the addition of real wastewater biomass (further details in Modrzyński, 2021). The packing of the columns was done under fully water saturated conditions to minimize the amount of trapped air during filling. A total of 6 sampling points were installed at each column: one at the inflow water headspace, four along the column (at 4, 8, 13 and 20 cm depth), and one at the outflow (30 cm depth), allowing the delineation of aqueous concentrations of ammonium, nitrate, nitrite, O_2, and dissolved organic carbon (DOC) at selected times at all six sampling ports.

At the end of the experiments of Modrzyński, 2021, the columns were dismantled and the sediment was characterized in terms of biofilm development from samples taken in all 10 columns at four different depths: in the reactive barrier, at zones around the first (depth A, 4 cm), second (depth B, 8 cm), and third sampling point (depth C, 13 cm), as well as at the interface between the reactive barrier and the silica coarse sand (depth O, 29 cm). For depths A, C and O, two samples per depth were taken, these integrating both the external and the internal parts of the column. For depth B, 3 samples were taken for the outer part of the column and 3 for the inner part of the column, in order to test if there were differences between them and if some kind of preferential heterogeneity could be observed. In each sediment sample, we measured the amount of glucose in the Extracellular Polymeric Substances (EPS), the non-soluble Organic Matter (associated to sedimentary organic matter and biological material), bacteria density in the sediment, and presence of algae (in the form of chlorophyll-a). Sediment samples of 3 ml (approximately 7 g) of sediments were stored frozen in plastic vials.

The sampling for bacterial analysis was also performed in drained sediment samples of 1 ml (2.3 g) from the columns, stored in glass vials with 10 ml of inlet water and 100 μl of a Formaldehyde solution at 37%, and stored in the fridge (unfrozen). For depths A, C and O, two samples integrating both the external and internal parts of the column were taken. No samples from depth B were taken in this case. Specific details of sampling and conservation procedures were identical as those in Perujo et al. (2019), based on the works of (Amalfitano et al., 2009; Amalfitano and Fazi, 2008).

2.4. Biogeochemical model set up

We constructed a numerical biogeochemical model using PHT3D v 2.17 (Prommer et al., 2001). This code couples the transport simulator MT3DMS (Zheng and Wang, 1999) and the geochemical code PHREEQC-2 (Parkhurst and Appelo, 2013), based on a sequential split-operator technique. The column experiments were modeled considering a 1D model with a total length of 29 cm (average of reactive barrier length for all the columns) divided in 100 cells of 0.29 cm with a width of 0.3419 m (in order to simulate the total surface of the column experiments assumed rectangular in the code). The model ran for 104 days (0.005 days for delta t), corresponding to the sampling period. The time discretization was selected to satisfy the Peclet and Courant numbers criteria. Dispersive transport was computed according to the third-order total variation diminishing scheme.

The conservative transport model with dual domain in PHT3D incorporated the parameters determined in the tracer test (see the next section). For the reactive part we incorporated the rates described in Table 1. For the reactions in equilibrium, they were taken directly from the general PHREEQC database. Kinetic processes (see Table 1)

Table 1
Stoichiometric relationships between the components of the biogeochemical reactions and processes rates, where $K_{max}' = /\gamma_i$. Here, we only shown the main compounds of the reaction. In DNRA we had no information in regard to the biomass yield between DNRA specific biomass and the stoichiometric reaction, therefore the stoichiometric reaction does not include that yield effect, however it does include the effect of biomass concentration (10% of total heterotrophic biomass for denitrification and 5% for DNRA, which are represented as alfa in the equations below). *Note that in the reaction rates, oxygen is considered O instead of O_2. This is intended, because the ipht3d model had oxygen in that notation, it is correctly converted in the reaction rates and onwards.

Process and reaction	*DOC*	CO_2	NH_4^+	NO_3^-	NO_2^-	N_2	H^+	O_2	HCO_3^-	*Compost*	BM_{het}	BM_{aut}	*Reaction rates**	
Nitrification (nitritation)			$0.1722\ NH_4^+ + 0.2223\ O_2 + 0.0055\ HCO_3^- \rightarrow 0.1666 NO_2^- + 0.60582\ H_2O + 0.333 H^+ + 0.0055\ C_5H_7O_2N$									+0.0055	$K_{'max,nit_1} \cdot \frac{[NH_4^+]}{[NH_4^+]+K_{s,NH_4^+}} \cdot \frac{[O]}{[O]+K_{s,O}} \cdot \frac{K_{i,NO_2^-}}{[NO_2^-]+K_{i,NO_2^-}} \cdot [BM_{aut}]$	(6)
	–	−0.0055	−0.1722	–	+0.1666	–	+0.333	−0.2223	−0.0055	–	–			
Nitrification (nitratation)			$0.503\ NO_2^- + 0.018\ CO_2 + 0.2271\ O_2 + 0.003\ H^+ + 0.010\ H_2O \rightarrow 0.5\ NO_3^- + 0.0035\ C_5H_7O_2N$									+0.0035	$K_{'max,nit_2} \cdot \frac{[NO_2^-]}{[NO_2^-]+K_{s,NO_2^-}} \cdot \frac{[O_2]}{[O_2]+K_{s,O}} \cdot \frac{K_{i,NO_3^-}}{[NO_3^-]+K_{i,NO_3^-}} \cdot [BM_{aut}]$	(7)
	–	−0.018	–	+0.5	−0.018	–	−0.003	−0.2271	–	–	–			
Aerobic oxidation of org. Matter			$0.25\ CH_2O + 0.1\ O_2 + 0.03\ HCO_3^- + 0.03\ NH_4^+ \rightarrow 0.22\ H_2O + 0.13\ CO_2 + 0.03\ C_5H_7O_2N$									+0.03	$K_{'max,DOC} \cdot \frac{[DOC]}{[DOC]+K_{s,DOC}} \cdot \frac{[O]}{[O]+K_{s,O}} \cdot [BM_{het}]$	(8)
	−0.25	+0.13	+0.03	–	–	–	–	−0.1	−0.03	–	–			
Compost release (fitted)	+0.9	–	+0.1	–	–	–	–	–	–	-1	–	–	$r'_{max} \cdot [Compost]$	(9)
Denitrification (nitrate reduction)			$0.2679\ NO_3^- + 0.0179\ H^+ + 0.25\ CH_2O \rightarrow 0.1607\ CO_2 + 0.1964286\ H_2O + 025\ NO_2^- + 0.01786\ C_5H_7O_2N$										$K_{'max,denit_1} \cdot \frac{[DOC]}{[DOC]+K_{s,DOC}} \cdot \frac{[NO_3^-]}{[NO_3^-]+K_{s,NO3-}} \cdot \frac{K'_{i,O}}{[O]+K'_{i,O_2}} \cdot \alpha_1 [BM_{het}]$	(11)
	−0.25	+0.161	–	−0.2679	+0.25	–	−0.018	–	–	–	+ 0.01786	–		
Denitrification (nitrite reduction)			$0.1859\ NO_2^- + 0.1859\ H^+ + 0.25\ CH_2O \rightarrow 0.15385\ CO_2 + 0.01923\ C_5H_7O_2N + 0.27564\ H_2O + 0.16667\ N_2$										$K_{'max,denit_2} \cdot \frac{[DOC]}{[DOC]+K'_{s,DOC}} \cdot \frac{[NO_2^-]}{[NO_2^-]+K_{s,NO2-}} \cdot \frac{K'_{i,NO_3^-}}{[NO_3^-]+K'_{i,NO_3^-}} \cdot \frac{K'_{i,O}}{[O]+K'_{i,O_2}} \alpha_1 [BM_{het}]$	(12)
	−0.25	+0.154	–	–	−0.186	+0.167	−0.186	–	–	–	+0.16667	–		
Dissimilatory Nitrate Reduction to ammonia (DNRA)			$2\ CH_2O + 1\ NO_3^- \rightarrow 1\ NH_4^+ + 2\ CO_2$										$K_{'max,DNRA} \cdot \frac{[DOC]}{[DOC]+K'_{s,DOC}} \cdot \frac{[NO_3^-]}{[NO_3^-]+K'_{s,NO3-}} \cdot \frac{K'_{i,O}}{[O_2]+K'_{i,O_2}} \alpha_2 [BM_{het}]$	(13)
	−2	+2	+1	−1	–	–	–	–	–	–	–	–		
Autotrophic biomass decay	–	–	–	–	–	–	–	–	–	–	–	−1	$b_{aut}[BM_{aut}]$	(14)
Heterotrophic biomass decay	–	–	–	–	–	–	–	–	–	–	−1	–	$b_{het}[BM_{het}]$	(15)

Table 2
Composition of the reactive layer in terms of percentages (in volume) of vegetal compost and sand. Each column was run in duplicate and inoculated. Column 1 and 2 were also run without inoculum in order to evaluate its effect.

Column notation	Proportion (%) compost/sand
1	0/100 (pure sand)
2	10–90
3	50–50
4	0/100 (pure sand)
5	10–90

were incorporated into the module in the form of BASIC routines, as explained in Rodríguez-Escales et al., 2016 and Carrey et al., 2018.

The experiment had four distinctive sub-periods in terms of signature of the inlet water. The chemical signature of the water in these sub-periods is described in Table 3. These values were used as input concentrations for the numerical model.

The calibration process of the biogeochemical model was performed manually (first considering data from the literature, then focusing on one biogeochemical process at a time and then going for another process until the iterative process yielded global good results), using the experimental concentration data for ammonium, nitrite, nitrate and DOCat the outflow of the columns and in the experimental profiles performed. For the calibration we considered the duplicates of the experiments.

3. Results and discussion

3.1. Conservative transport and biofilm growth: evaluating the evolution of hydrological parameters

At the beginning and at the end of the column experiments a conservative tracer test was performed in order to characterize the apparent transport properties of the columns, and in particular to test the impact of biofilm growth in the columns upon transport of conservative species. The tracer selected was tritium; it was instantaneously injected using a laboratory syringe in the stagnant zone of each column, and monitored continuously at the outflow of the column, thus being able to reconstruct the breakthrough curves (BTCs). For more details about the experimental procedure and analysis of the tracer test, see Modrzyński, 2021.

Table 3
Chemical signature of the injected water (in mol/L) for the four sub-periods. (*) DIC - Dissolved Inorganic Carbon; (**) DOC - Dissolved Organic Carbon; (***) these values are 15% higher than the experimental concentration in Modrzyński et al. (2020), in order to correctly fit the experimental data with the numerical model. Compost and the two elements representing biomass are considered solid species and their concentrations are related to the porosity of the media.

Compounds	Sub-period – I days 0 to 5	Sub-period – II days 5 to 19	Sub-period – III days 19 to 29	Sub-period – IV days 29 to 116
NH_4^+ (M)	6.43×10^{-4}	6.43×10^{-4}	1.60×10^{-4} ***	1.60×10^{-4}***
DIC* (M)	3.00×10^{-3}	3.00×10^{-3}	3.00×10^{-3}	3.00×10^{-3}
Ca (M)	2.00×10^{-3}	2.00×10^{-3}	2.00×10^{-3}	2.00×10^{-3}
Cl (M)	1.30×10^{-2}	1.30×10^{-2}	1.30×10^{-2}	1.30×10^{-2}
DOC** (M)	2.34×10^{-3}	8.83×10^{-4}	2.79×10^{-4}	3.92×10^{-4}
K (M)	6.00×10^{-4}	6.00×10^{-4}	6.00×10^{-4}	6.00×10^{-4}
Mg (M)	1.50×10^{-3}	1.50×10^{-3}	1.50×10^{-3}	1.50×10^{-3}
Na (M)	1.00×10^{-2}	1.00×10^{-2}	1.00×10^{-2}	1.00×10^{-2}
O_2 (M)	3.15×10^{-4}	3.15×10^{-4}	3.15×10^{-4}	3.15×10^{-4}
SO_4^{-2} (M)	1.5×10^{-3}	1.5×10^{-3}	1.5×10^{-3}	1.5×10^{-3}
pH	6.4	6.4	6.4	6.4
Pe	14.265	14.265	14.265	14.265
Biomass (het) (M)	8.00×10^{-6}			
Biomass (auto) (M)	1.00×10^{-6}			
Compost (M)	100% sand	–		
	10% comp	0.010		
	50% comp	0.053		

Table 4
Apparent transport parameters determined from the tracer tests including their standard error.

	Units	Column 1: 100% sand		Column 2: 10% compost		Column 3: 50% compost	
		Initial	End	Initial	End	Initial	End
Flow rate	ml/min	0.5	0.5	0.5	0.5	0.5	0.5
Water velocity	cm/min	0.0344	0.039	0.031	0.035	0.028	0.029
Dispersivity	cm	0.040 ± 0.009	0.037 ± 0.016	0.219 ± 0.103	0.194 ± 0.075	0.762 ± 0.099	0.724 ± 0.724
ϕ_T	[−]	0.424	0.366	0.471	0.424	0.518	0.504
ϕ_{im}	[−]	0.028 ± 0.011	0.037 ± 0.046	0.021 ± 0.228	0.030 ± 0.190	0.031 ± 0.159	0.146 ± 0.151
β	[−]	0.071 ± 0.030	0.111 ± 0.148	0.047 ± 0.529	0.076 ± 0.510	0.064 ± 0.349	0.408 ± 0.596
α	min^{-1}	0.125 ± 0.025	$0.1597 \pm 7.4 \times 10^{-3}$	0.0492 ± 0.013	0.068 ± 0.0255	$0.0081 \pm 1.28 \times 10^{-5}$	$0.1403 \pm 1.96 \times 10^{-4}$

While the tests performed prior to the experiments could mostly be interpreted using the traditional Advection Dispersion Equation (ADE), we preferred to interpret all tests using a common model, being the dual domain, to allow comparison of hydraulic parameters between …. The experimental BTC data was fitted using the CXTFIT code (Toride et al., 1995); the parameters fitted were: dispersivity; total, mobile and immobile porosities; and mass transfer coefficient (Table 4, showing the mean value and the standard deviation of the calibrated parameters).

Regardless the initial values, after the four months of the experiment, the fitted immobile porosity changed significantly (Fig. 2 and Table 4), mostly in the columns containing compost. On the contrary, no significant influence of inoculation on hydraulic parameters was observed (results not shown). For this reason, data corresponding to non-inoculated columns were included as additional replicates of columns 1 and 2, respectively (see Table 2).

Non-Fickianity in the curves increases with β ($\beta = 0$ corresponding to pure Fickian behaviour). For all three experiments we observed a significant increase of the fraction of immobile porosity from the initial tracer experiments (displaying very low β values), to those performed once the experiments were completed. The effect is most significant in the column containing 50% proportion of compost. Enhanced tailing in all columns after day 104 is also modeled by (relatively similar for all columns) values of the mass-transfer rates (α). Tailing is associated with the changes in the ecosystem of the microorganisms (quantitatively and qualitatively) colonizing the columns as observed in other works (Rodríguez-Escales et al., 2016; Rubol et al., 2014). The α values in the colonized columns reported in Table 4 indicate residence times of the tracer within the biofilm on the order of 6–15 min, consistent with the value reported by Sanchez-Vila and Rodriguez-Escales (submitted) of 5 min as overall representative of similar experiments performed worldwide.

Data corresponding to bacterial density in the sediment correlates significantly with the percentage of compost and β (Fig. 3a). Bacterial density was correlated with the compost content, with 20–25 × 10^7, 5–10 × 10^7, and 2–3 × 10^7 cells per g_{DW} for 50%, 10% and 0% compost, respectively. This suggests the compost enhances bacterial growth in the system leading to the variation in the hydrological transport parameters.

Noteworthy, the peaks of bacterial density correspond to the first centimetres of the column. We associate this observation to differences in bacterial growth, known to be much higher in aerobic conditions as compared to anaerobic since oxygen, being the electron acceptor,

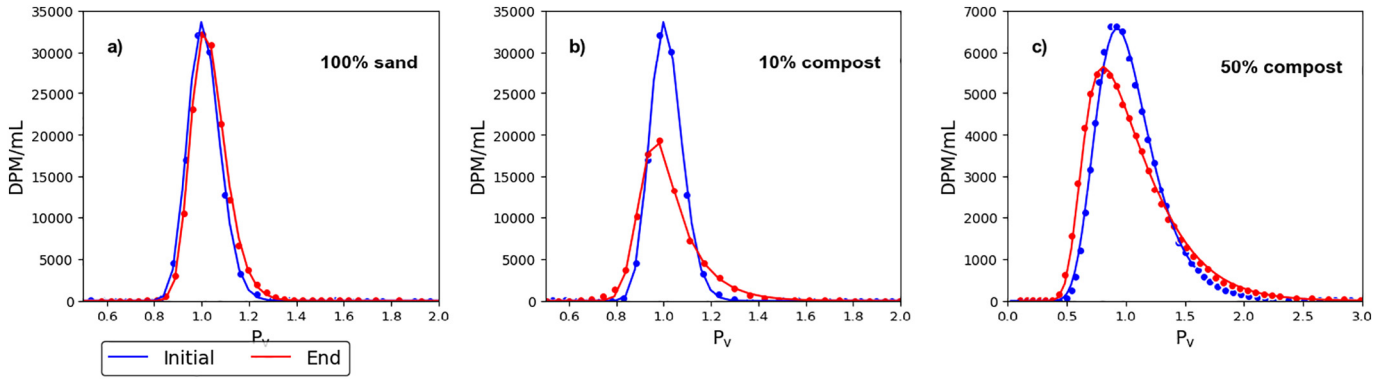

Fig. 2. Breakthrough curves of the tracer tests performed at the beginning (day 0) and the end of the experiments (day 116). The points represent the experimental concentration of tritium recorded whereas the lines are the model results. Column notation is displayed in Table 2.

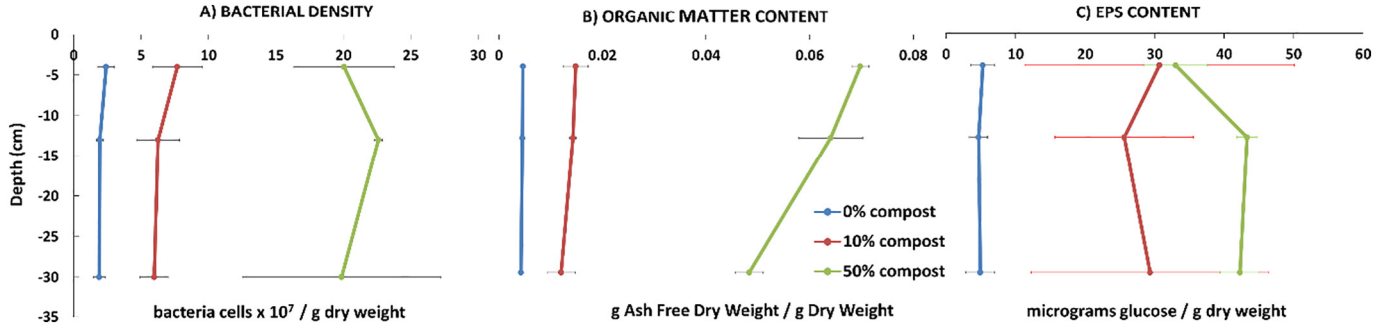

Fig. 3. Bacterial density, solid organic matter and EPS content in different depths, the error bars denote the standard deviation between the samples from each column setup.

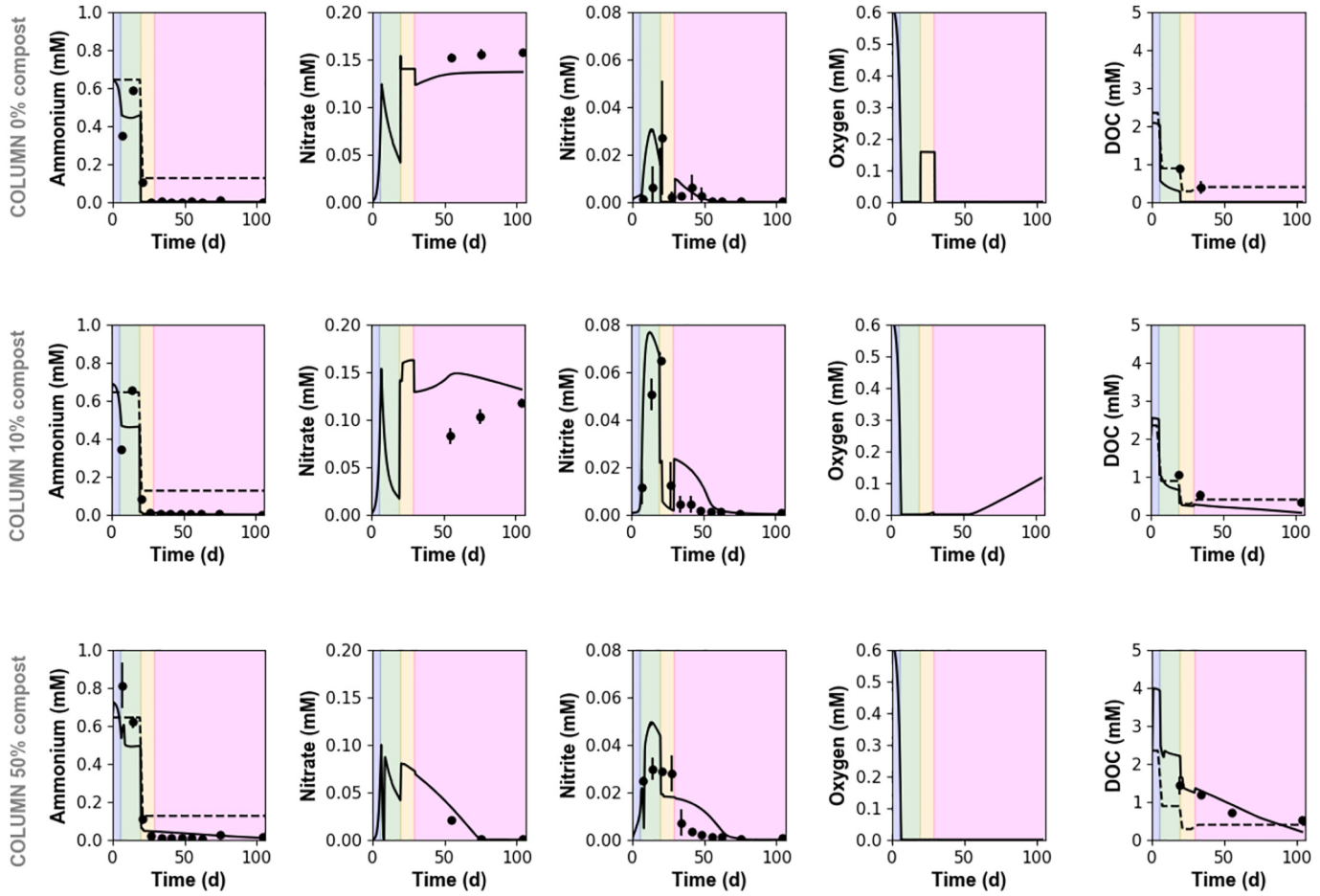

Fig. 4. Results of the biogeochemical modeling at the outflow of the different columns. Black points indicate experimental data whereas black solid lines are the model results. Dashed black lines represent the respective concentrations at the inlet. Background colors of the plots refer to the different Inflow sub-periods (Table 3) in the experiment: blue – I, green – II, yellow – III, red – IV.

provides much better energy yield than most electron acceptors (in addition to having a biomass growth yield higher than anaerobic bacteria). Only to be followed closely by nitrate energy yield, which is the reason why this compound is used in those environments where oxygen availability is low (Rittmann and McCarty, 2012). On the other hand, as the content of chlorophyll-a was negligible, the growth of biomass was not associated to photosynthetic metabolism (in addition the columns were covered in aluminium foil to prevent light penetration).

The change in transport properties during the experiments is also reflected in the biological variables measured at day 104 for different depths (4, 8 and 25 cm) (see Fig. 3). The content of non-soluble organic matter (0.5% in 100% sand columns, 1.0–1.5% in 10% compost columns, 5–7% in 50% compost columns, Fig. 3) increased with the percentage of compost mixed with sand. Note that in compost columns a decrease of non-soluble organic matter in depth was observed in Fig. 4, whereas it remained constant in full sand columns. This was arguably associated to a potential release of soluble organic matter in columns that decreased over time and confirms the necessity of adding this process to the conceptual model displayed in Fig. 1. Furthermore, it would indicate limitation of the use of compost as a material in a reactive barrier has a limited lifetime, especially in terms of providing an extra source of dissolved organic carbon.

Finally, EPS quantity (measured as glucose) also correlated (for both cases p-value significantly low) positively with the proportion of compost (coefficient of determination r^2 = 0.81) and β (r^2 = 0.46) in Fig. 3c. However, the correlation due to β is subject to variation because the value of this parameter has a lot of variability in the data obtained (specially for the case of 0% compost). We associate this effect to the growth of biofilm favoured by the nutrients supplied by the compost and the addition of microorganisms already present in the compost, again consistent with the reported changes in transport parameters.

Therefore, after combining the data from tritium BTCs and biological analysis, the question that arises is whether the addition of compost on the top soil of an aquifer forming a reactive barrier is overall beneficial when combining quantitative and qualitative aspects. So far, the impact on infiltration dynamics, reducing total infiltration capacity and enhancing non-Fickian transport caused by biofilm expansion in the pore network is clear, increasing with compost content and time. However, the indirect impact of biofilm growth is quite complex. The presence of compost enhances biological activity. This agrees with surface infiltration experimental information in field scale studies, where biofilm needs to be scraped, treated or dried repeatedly to sustain the infiltration yields over time (Dillon et al., 2019, 2009). Such enhanced biological activity affects geochemical reactions catalysed by microorganisms, resulting in a significant transformation of the water quality. In the following section, we will evaluate the impact of such transformation upon the N and C cycles.

3.2. Biogeochemical modeling: evaluating the impact of a reactive layer in the carbon and nitrogen cycles

The biogeochemical model described in Fig. 1 is used to simulate the breakthrough curves (BTCs) at the outflow of the column (Fig. 4) and the depth profiles alongside the columns (supporting information Figs. S1, S2 and S3). Fig. 4 presents both the experimental data and the best fitted model using the parameters listed in Table 5. Profile data at

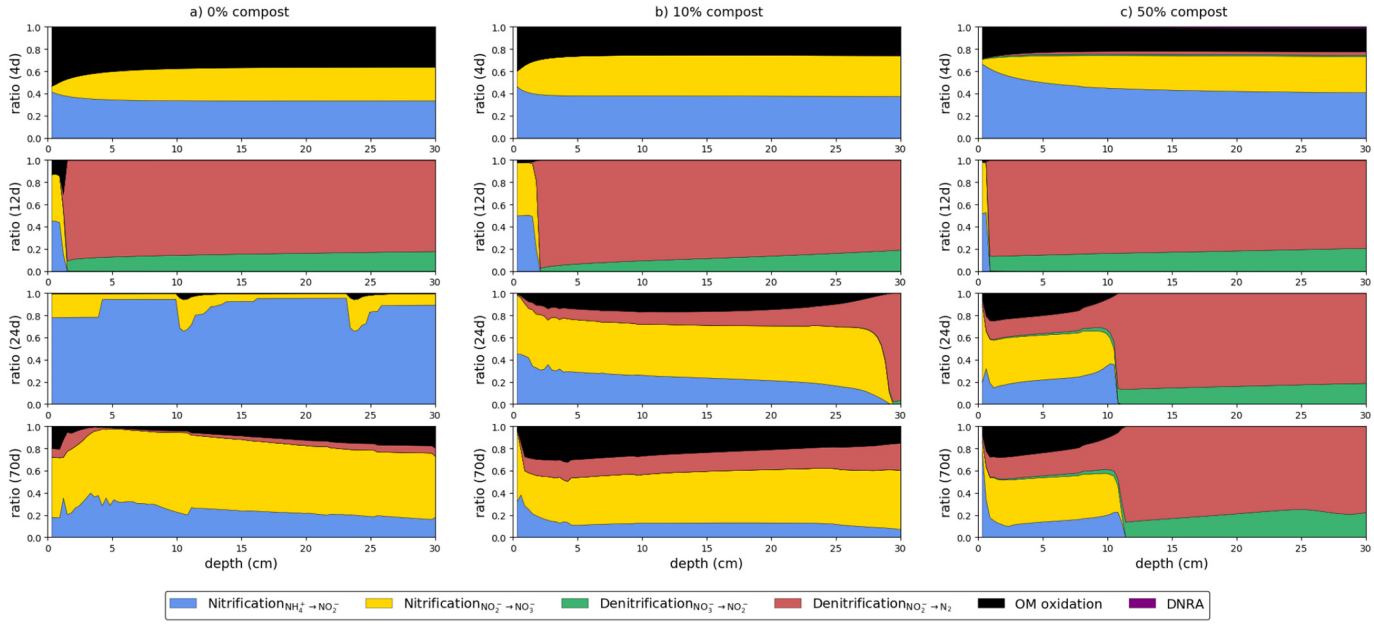

Fig. 5. Kinetic rates profiles for the three column setups, including data from the four sub-periods modeled (days 4, 12, 24 and 70 respectively for sub-periods I to IV). The days selected in the graphs were approximately at the middle of each sub-period (Table 3).

selected times are presented in the Supporting Information (Figs. S1, S2 and S3). In general, the model is well adjusted to the experimental data. In order to understand relative importance of the different processes, we studied the evolution of rates presented in Fig. 5.

In sub-period I (days 0 to 5), nitrification was the dominating process, indicated by the high concentrations of ammonia and oxygen in all the column systems (Figs. 4 and 5). However, there was not enough oxygen to exhaust ammonia and organic carbon. Columns with 10% compost and even more that with 50% compost, showed the activation of DNRA activity, due to the increase of organic carbon release from the compost. Focusing on the relative importance of different process rates (Fig. 5), we found that nitrification, organic carbon oxidation and compost release (in columns 2 and 3) showed the highest rates. Besides, due to the short time and high concentrations of oxygen, organic carbon and ammonia, inhibition and saturation terms embedded in the expressions for rates were not significant, so that data could be fitted as well using simple first-order degradation rates, governed by K'_{max}. For this same reason, the estimated inhibition or saturation constants are highly uncertain.

Sub-period II (days 5 to 19) was characterized by the increasing effect of denitrification due to the previous consumption of oxygen and the presence of generation of nitrate from nitrification. This was especially true in the profiles corresponding to day 7 (bottom half) and day 14 (all the column) that show the lack of oxygen (Figs. S1, S2 and S3 from the supporting information). In this sub-period the inlet concentration of organic carbon was significantly reduced (from 2.3 to 0.88 mM), which could explain the nitrite accumulation associated to denitrification (Betlach and Tiedje, 1981) in addition to the accumulation due to incomplete nitrification. This accumulation, present in all columns, was most significant in those including a fraction of compost. Indeed, in the column with 10% compost, the concentration of nitrite had a peak exceeding the drinking water standard (WHO, 2008). Thus, it would seem that the presence of a reactive layer in infiltration facilities could lead to transient accumulations of nitrite. Besides denitrification, a significant process in this sub-period was the presence of DNRA (mostly in the column with 50% compost, see Fig. 5) due to the higher effect of organic carbon in compost release. Note that DNRA processes are short lived, not only because they require a high concentration of organic carbon, but because they need nitrate as their input, competing directly with denitrification (see Fig. 5). The kinetics of DNRA are required to take as much nitrate as possible but only until a certain amount of organic matter (1×10^{-3} mM approximately due to the Ks of organic matter with a value of 2.8×10^{-4} M), guaranteeing that DNRA only occurred at the beginning of the column experiment in agreement with the experimental data.

Sub-period III (days 19 to 29) was defined by a sharp decrease in the inlet concentrations of both ammonia (reducing from 0.64 to 0.16 mM) and organic carbon (from 0.88 to 0.28 mM). Under these conditions of limited electron donor concentrations, oxidation of organic carbon, denitrification and DNRA were significantly hindered. In the 100% sand column, the concentration of organic carbon was below the K_s and therefore the reactions barely took place (Fig. 5), and consequently the concentration of oxygen eventually increased enough to generate aerobic conditions. On the other hand, columns with a fraction of compost still had a significant release of organic matter and therefore the organic carbon concentrations were not below the K_s level and denitrification was still present. Overall, nitrification regained more importance, reducing nitrite and increasing nitrate concentrations.

Sub-period IV (days 29 to 116) maintained the same ammonia concentration as sub-period III, but with a slight raise in the organic matter concentration (from 0.28 to 0.39 mM). This had relatively no effect on the 100% sand column because the main process was still nitrification (accumulating nitrate). This was fully observed in the profiles for all columns, displaying an increase in nitrate concentration with depth, indicating that there was not enough organic matter to have a significant effect of denitrification at these final sub-periods. However, in columns with compost, denitrification was more significant, causing an accumulation of nitrite, consistent with both experimental data and the fitted K_s value of organic carbon (see Table 4). In the 50% compost column, nitrite accumulation indicated incomplete denitrification. This observation was also confirmed in the profiles, where at the top half of the column nitrification was quite present (high nitrate concentrations), while at the bottom half complete denitrification occurred (fully consuming both nitrate and nitrite, see Figs. 4 and 5).

The kinetic of nitrification and aerobic oxidation of organic carbon are in general similar (within the same order of magnitude) for all the columns (Table 5). Denitrification, on the other hand, implied significant differences in the calibrated K_s values, indicating that the larger the fraction of compost, the higher the tendency to consume respective substrates. Inhibition, can be fitted with similar values for all reactions

Table 5
Fitted parameters from biogeochemical modeling. Literature data obtained from Gao et al., 2010; Dinçer and Kargi, 2000; MacQuarrie and Sudicky, 2001; Lee et al., 2006.

	Units	Column 100% sand	Column 10% compost	Column 50% compost	Literature
Nitrification (oxidation of ammonium)					
$K_{max,\ nit_1}{}'$	d^{-1}	4.234	3.715	4.579	1–100
$K_{s,\ O}$	M	1.3×10^{-5}	5×10^{-6}	1×10^{-6}	6.25×10^{-6}–4.812×10^{-5}
$K_{s,\ NH_4^+}$	M	1×10^{-5}	1×10^{-5}	1×10^{-5}	7.143×10^{-6}–3.571×10^{-4}
$K_{I,\ NO_2^-}$	M	4×10^{-5}	8×10^{-5}	4×10^{-5}	NF
Nitrification (oxidation of nitrite)					
$K_{max,\ nit_2}{}'$	$S^{-1}(d^{-1})$	10.368	8.64	8.64	1–100
$K_{s,\ O}{}'$	M	1×10^{-6}	1×10^{-6}	1×10^{-5}	6.25×10^{-6}–4.812×10^{-5}
$K_{s,\ NO_2^-}$	M	4×10^{-6}	1×10^{-6}	1×10^{-5}	7.143×10^{-6}–3.571×10^{-4}
$K_{I,\ NO_3^-}$	M	2×10^{-4}	1×10^{-4}	1.7×10^{-4}	NF
Aerobic oxidation of organic matter					
$K_{max,\ DOC}{}'$	$S^{-1}(d^{-1})$	0.9504	0.864	0.8208	1–100
$K_{s,\ O}{}''$	M	1×10^{-6}	1×10^{-5}	2×10^{-5}	6.25×10^{-6}–4.812×10^{-5}
$K_{s,\ DOC}$	M	9×10^{-5}	4×10^{-4}	2.8×10^{-4}	8.33×10^{-6}–3.33×10^{-3}
Denitrification (reduction of nitrate)					
$K_{max,\ denit_1}{}'$	$S^{-1}(d^{-1})$	2.592	9.936	3.9744	0.2–40
$K_{s,\ NO_3^-}$	M	1×10^{-4}	5×10^{-5}	1×10^{-6}	7.143×10^{-6}–3.571×10^{-4}
$K'_{s,\ DOC}$	M	1×10^{-5}	7×10^{-5}	5×10^{-6}	8.3167×10^{-4}
$K_{I,\ O}$	M	5×10^{-6}	2×10^{-5}	1×10^{-4}	NF
Denitrification (reduction of nitrite)					
$K_{max,\ denit_2}{}'$	$S^{-1}(d^{-1})$	0.39744	2.16	2.2464	0.2–40
$K'_{s,\ NO_2^-}$	M	1×10^{-6}	2×10^{-5}	1×10^{-6}	NF
$K''_{s,\ DOCc}$	M	6×10^{-5}	2×10^{-4}	1×10^{-5}	8.3167×10^{-4}
$K'_{I,\ O}$	M	9×10^{-5}	7×10^{-5}	9×10^{-5}	NF
$K'_{I,\ NO_3^-}$	M	2×10^{-4}	1.5×10^{-4}	6×10^{-5}	NF
DNRA					
$K_{max,\ DNRA}{}'$	$S^{-1}(d^{-1})$	–	–	82.08	NF
$K'_{s,\ NO_3^-}$	M	–	–	2×10^{-5}	NF
$K''''_{s,\ DOC}$	M	–	–	2.8×10^{-4}	NF
$K''_{I,\ O}$	M	–	–	6×10^{-6}	NF
Growth and decay of autotrophic biomass					
$Y_{ox\ amm}$	M_{auto}/M	0.16	0.16	0.16	0.2–0.3
$Y_{ox\ nitit}$	M_{auto}/M	0.035	0.035	0.035	NF
b_{aut}	d^{-1}	1×10^{-8}	1×10^{-8}	1×10^{-8}	0.02–0.06
Growth and decay of heterotrophic biomass					
$Y_{ox\ DOC}$	M_{hetero}/M	0.6	0.6	0.6	NF
$Y_{denitit}$	M_{hetero}/M	0.035	0.035	0.035	NF
$Y_{denitat}$	M_{hetero}/M	0.038	0.038	0.038	NF
b_{het}	d^{-1}	1×10^{-8}	1×10^{-8}	1×10^{-8}	NF
Y_{DNRA}	M_{hetero}/M	–	–	0.01	NF
Release compost					
K	$S^{-1}(d^{-1})$	–	8.64×10^{-5}	2.6784×10^{-4}	NF

(except for denitrification reduction of nitrate in the nitrate inhibition), probably because this process was hardly activated during the relatively short duration of the experiment.

Generally, the evolution of the biogeochemical signature of the infiltrating water was affected by the inclusion of a source of labile organic carbon at the top surface of an aquifer in the form of a reactive barrier, significantly affects the fate of the different compounds involved in the nutrient (C, N) cycles, both short and long term. When the barrier contains compost, transient accumulations of nitrite can be observed together with an overall increase in nitrate concentrations, probably due to the oxidation of leached ammonia. This could pose a risk for aquifer nitrate pollution; yet, this is counteracted by the DOC leaching, favoring denitrification and nitrate reduction. Besides, adding a reactive layer increases the number and the intensity of bacterial processes occurring in the top layer of the barrier, increasing the variability of processes coexisting within a very thin layer (e.g. there is a clear transition from an oxic to an anoxic zone). In terms of purification capacity of MAR, this variability would increase the potential for degradation of some recalcitrant compounds (e.g., Emerging Organic Compounds) mostly occurring by co-metabolism (Dalton and Stirling, 1982; Rodríguez-Escales et al., 2017).

4. Conclusions

The presence of a compost reactive barrier placed on top of an infiltration pond used as a MAR facility has both pros and cons. In this work, we studied how addition of compost might influence both the infiltration rates (i.e. quantitative issues and sustainability), and the evolution in space and time of the quality of the infiltrating water. This was done by analyzing flow through column experiments, combined with biological analysis of the sediments once the columns were dismantled. Emphasis is placed in formulating a complex conceptual model of the fate of the different compounds that constitute the nutrient (C and N) cycles involved, and using this model to interpret the observations in the experiments reported by Modrzyński, 2021.

Overall, the potential of compost is to release labile organic carbon, enhancing biomass development and biofilm formation, and subsequently stimulate processes catalysed by the microorganisms. Therefore, the reactive barrier acts by reducing significantly the infiltration capacity of the system; the higher the compost percentage, the faster the growth of microorganisms and the reduced porosity, reducing overall saturated hydraulic conductivity, and enhancing dispersivity as observed in breakthrough curves of tracer tests. The combination of

compost with sand implies that this infiltration capacity reduction can be managed adequately by analyzing in the future optimal proportions of compost and sand, and including other materials, like wood chips or other more permeable materials. This analysis could be assessed by means of full integrated biogeochemical models once a few batch and column experiments are performed (to obtain the values specific of the local parameters) with local soil and compost in the study areas of interest to install future MAR facilities.

This reduction in infiltration is potentially compensated by the benefits in water treatment resulting in improved water quality. The larger the volume colonized by biofilm, usually means the larger the increase in bacterial activity, although and overgrowth of biofilm may be also harmful for these bacteria if nutrients are blocked from deeper parts of the biofilm. Such activity results in a pronounced enhancement of geochemical reactions, in particular those catalysed by microorganisms, such as nitrification, denitrification and organic matter oxidation. The addition of compost in the reactive barriers will have a significant impact on the nutrient dynamics: In the short run, the addition of compost caused leaching of nutrients (both carbon and nitrogen) and the occurrence of DNRA, while in the long run, the overall concentrations of nutrients (especially nitrogen) were the lowest of the three column setups. Finally, in terms of purification capacity of MAR systems, this variability would also increase the possibility of the degradation of recalcitrant compounds by co-metabolism.

To conclude, there is a need to look at MAR from an integrated point of view, balancing the quantitative with the qualitative aspects. This will allow maximizing the overall benefits of recharging aquifers with treated wastewater, rather than having to rely on excessively high-quality water for recharge. Eventually, this can expand the potential of MAR in providing water security in the changing climate.

Supplementary data to this article can be found online at https://doi.org/10.1016/j.scitotenv.2021.145490.

CRediT authorship contribution statement

Arnau Canelles: Conceptualization, Methodology, Software, Validation, Formal analysis, Writing – original draft, Writing – review & editing. **Paula Rodríguez-Escales:** Conceptualization, Methodology, Software, Validation, Formal analysis, Writing – original draft, Supervision, Funding acquisition. **Jakub Jan Modrzyński:** Investigation, Resources. **Christian Albers:** Investigation, Resources. **Xavier Sanchez-Vila:** Formal analysis, Writing – original draft, Writing – review & editing, Supervision, Funding acquisition.

Declaration of competing interest

The authors declare that they have no known competing financial interests or personal relationships that could have appeared to influence the work reported in this paper.

Acknowledgements

This work was financially supported by the EU project ACWAPUR (Water JPI - WaterWorks 2014 code PCIN-2015-239), the Spanish University Professor Formation program FPU (Ministerio de Ciencia, Innovación y Universidades code FPU17/05031), MONOPOLIOS (RTI2018-101990-B-100, MINECO/FEDER), the EU project MARADENTRO (PCI2019-103425-WW2017), the Catalan Research Project RESTORA (ACA210/18/00040) and AGAUR (AQU - 2017 SGR 1485).

References

Akhavan, M., Imhoff, P.T., Andres, A.S., Finsterle, S., 2013. Model evaluation of denitrification under rapid infiltration basin systems. J. Contam. Hydrol. 152, 18–34. https://doi.org/10.1016/j.jconhyd.2013.05.007.

Alazard, M., Boisson, A., Maréchal, J.C., Perrin, J., Dewandel, B., Schwarz, T., Pettenati, M., Picot-Colbeaux, G., Kloppman, W., Ahmed, S., 2016. Etude de la dynamique et des écoulements dans un aquifère cristallin fracturé en zone semi-aride (Inde) à partir de données de forage: conséquences pour la recharge artificielle des aquifères. Hydrogeol. J. 24, 35–57. https://doi.org/10.1007/s10040-015-1323-5.

Amalfitano, S., Fazi, S., 2008. Recovery and quantification of bacterial cells associated with streambed sediments. J. Microbiol. Methods 75, 237–243. https://doi.org/10.1016/j.mimet.2008.06.004.

Amalfitano, S., Puddu, A., Fazi, S., 2009. Flow cytometric analysis of benthic prokaryotes attached to sediment particles. J. Microbiol. Methods 79, 246–249. https://doi.org/10.1016/j.mimet.2009.09.005.

Barba, C., Folch, A., Sanchez-Vila, X., Martínez-Alonso, M., Gaju, N., 2019. Are dominant microbial sub-surface communities affected by water quality and soil characteristics? J. Environ. Manag. 237, 332–343. https://doi.org/10.1016/j.jenvman.2019.02.079.

van den Berg, E.M., Boleij, M., Kuenen, J.G., Kleerebezem, R., van Loosdrecht, M.C.M., 2016. DNRA and denitrification coexist over a broad range of acetate/N-NO3- ratios, in a chemostat enrichment culture. Front. Microbiol. 7, 1842. https://doi.org/10.3389/fmicb.2016.01842.

Betlach, M.R., Tiedje, J.M., 1981. Kinetic explanation for accumulation of nitrite, nitric oxide, and nitrous oxide during bacterial denitrification †. Appl. Environ. Microbiol. 42, 1074–1084. https://doi.org/10.1128/aem.42.6.1074-1084.1981.

Carles Brangarí, A., Sanchez-Vila, X., Freixa, A., M. Romaní, A., Rubol, S., Fernàndez-Garcia, D., 2017. A mechanistic model (BCC-PSSICO) to predict changes in the hydraulic properties for bio-amended variably saturated soils. Water Resour. Res. 53, 93–109. https://doi.org/10.1002/2015WR018517.

Carrey, R., Rodríguez-Escales, P., Soler, A., Otero, N., 2018. Tracing the role of endogenous carbon in denitrification using wine industry by-product as an external electron donor: coupling isotopic tools with mathematical modeling. J. Environ. Manag. 207, 105–115. https://doi.org/10.1016/j.jenvman.2017.10.063.

Dalton, H., Stirling, D.I., 1982. Co-metabolism. Philos. Trans. R. Soc. Lond. Ser. B Biol. Sci. 297, 481–496. https://doi.org/10.1098/rstb.1982.0056.

Delay, F., Porel, G., Chatelier, M., 2013. A dual flowing continuum approach to model denitrification experiments in porous media colonized by biofilms. J. Contam. Hydrol. 150, 12–24. https://doi.org/10.1016/j.jconhyd.2013.04.001.

Dillon, P., Pavelic, P., Page, D., Beringen, H., Ward, J., 2009. Managed Aquifer Recharge: An Introduction. Waterlines Report Series Canberra.

Dillon, P., Toze, S., Page, D., Vanderzalm, J., Bekele, E., Sidhu, J., Rinck-Pfeiffer, S., 2010. Managed aquifer recharge: rediscovering nature as a leading edge technology. Water Sci. Technol. 62, 2338–2345. https://doi.org/10.2166/wst.2010.444.

Dillon, P., Stuyfzand, P., Grischek, T., Lluria, M., Pyne, R.D.G., Jain, R.C., Bear, J., Schwarz, J., Wang, W., Fernandez, E., Stefan, C., Pettenati, M., van der Gun, J., Sprenger, C., Massmann, G., Scanlon, B.R., Xanke, J., Jokela, P., Zheng, Y., Rossetto, R., Shamrukh, M., Pavelic, P., Murray, E., Ross, A., Bonilla Valverde, J.P., Palma Nava, A., Ansems, N., Posavec, K., Ha, K., Martin, R., Sapiano, M., 2019. Sixty years of global progress in managed aquifer recharge. Hydrogeol. J. 27, 1–30. https://doi.org/10.1007/s10040-018-1841-z.

Dinçer, A.R., Kargi, F., 2000. Kinetics of sequential nitrification and denitrification processes. Enzym. Microb. Technol. 27, 37–42. https://doi.org/10.1016/S0141-0229(00)00145-9.

Fernàndez-Garcia, D., Sanchez-Vila, X., 2015. Mathematical equivalence between time-dependent single-rate and multirate mass transfer models. Water Resour. Res. 51, 3166–3180. https://doi.org/10.1002/2014WR016348.

Ganot, Y., Holtzman, R., Weisbrod, N., Bernstein, A., Siebner, H., Katz, Y., Kurtzman, D., 2018. Managed aquifer recharge with reverse-osmosis desalinated seawater: modeling the spreading in groundwater using stable water isotopes. Hydrol. Earth Syst. Sci. 22, 6323–6333. https://doi.org/10.5194/hess-22-6323-2018.

Gao, D., Peng, Y., Wu, W.M., 2010. Kinetic model for biological nitrogen removal using shortcut nitrification-denitrification process in sequencing batch reactor. Environ. Sci. Technol. 44, 5015–5021. https://doi.org/10.1021/es100514x.

Gibert, O., Pomierny, S., Rowe, I., Kalin, R.M., 2008. Selection of organic substrates as potential reactive materials for use in a denitrification permeable reactive barrier (PRB). Bioresour. Technol. 99, 7587–7596. https://doi.org/10.1016/j.biortech.2008.02.012.

Giorgi, F., Lionello, P., 2007. Climate Change Projections for the Mediterranean Region. https://doi.org/10.1016/j.gloplacha.2007.09.005.

Grau-Martínez, A., Torrentó, C., Carrey, R., Rodríguez-Escales, P., Domènech, C., Ghiglieri, G., Soler, A., Otero, N., 2017. Feasibility of two low-cost organic substrates for inducing denitrification in artificial recharge ponds: batch and flow-through experiments. J. Contam. Hydrol. 198, 48–58. https://doi.org/10.1016/j.jconhyd.2017.01.001.

Grau-Martínez, A., Folch, A., Torrentó, C., Valhondo, C., Barba, C., Domènech, C., Soler, A., Otero, N., 2018. Monitoring induced denitrification during managed aquifer recharge in an infiltration pond. J. Hydrol. 561, 123–135. https://doi.org/10.1016/j.jhydrol.2018.03.044.

Green, C.T., Puckett, L.J., Böhlke, J.K., Bekins, B.A., Phillips, S.P., Kauffman, L.J., Denver, J.M., Johnson, H.M., 2008. Limited occurrence of denitrification in four shallow aquifers in agricultural areas of the United States. J. Environ. Qual. 37, 994–1009. https://doi.org/10.2134/jeq2006.0419.

Haggerty, R., Gorelick, S.M., 1995. Multiple-rate mass transfer for modeling diffusion and surface reactions in media with pore-scale heterogeneity. Water Resour. Res. 31, 2383–2400. https://doi.org/10.1029/95WR10583.

IPCC, 2007. IPCC Climate Change: The Physical Science Basis, IPCC Climate Change: The Physical Science Basis.

Koper, T.E., Stark, J.M., Habteselassie, M.Y., Norton, J.M., 2010. Nitrification exhibits Haldane kinetics in an agricultural soil treated with ammonium sulfate or dairy-waste compost. FEMS Microbiol. Ecol. 74, 316–322. https://doi.org/10.1111/j.1574-6941.2010.00960.x.

Lawrence, A.E., Sanchez-Vila, X., Rubin, Y., 2002. Conditional moments of the breakthrough curves of kinetically sorbing solute in heterogeneous porous media using multirate mass transfer models for sorption and desorption. Water Resour. Res. 38. https://doi.org/10.1029/2001wr001006 30-1-30–12.

Lee, M.S., Lee, K.K., Hyun, Y., Clement, T.P., Hamilton, D., 2006. Nitrogen transformation and transport modeling in groundwater aquifers. Ecol. Model. 192, 143–159. https://doi.org/10.1016/j.ecolmodel.2005.07.013.

MacQuarrie, K.T.B., Sudicky, E.A., 2001. Multicomponent simulation of wastewater-derived nitrogen and carbon in shallow unconfined aquifers - I. Model formulation and performance. J. Contam. Hydrol. 47, 53–84. https://doi.org/10.1016/S0169-7722(00)00137-6.

Maeng, S.K., Sharma, S.K., Lekkerkerker-Teunissen, K., Amy, G.L., 2011. Occurrence and fate of bulk organic matter and pharmaceutically active compounds in managed aquifer recharge: a review. Water Res. 45, 3015–3033. https://doi.org/10.1016/j.watres.2011.02.017.

Maliva, R.G., Missimer, T.M., 2012. Arid lands water evaluation and management. Environ. Sci. Eng. https://doi.org/10.1007/978-3-540-88258-9.

Mastrocicco, M., Colombani, N., Salemi, E., Castaldelli, G., 2011. Reactive modeling of denitrification in soils with natural and depleted organic matter. Water Air Soil Pollut. 222, 205–215. https://doi.org/10.1007/s11270-011-0817-6.

Miller, J.H., Ela, W.P., Lansey, K.E., Chipello, P.L., Arnold, R.G., 2006. Nitrogen transformations during soil-aquifer treatment of wastewater effluent - oxygen effects in field studies. J. Environ. Eng. 132, 1298–1306. https://doi.org/10.1061/(ASCE)0733-9372(2006)132:10(1298).

Modrzyński, J.J., 2020. Combined removal of organic micropollutants and ammonium during managed aquifer recharge - a column study to disclose processes in reactive barriers. ter Res.

Modrzyński, J.J., 2021. Combined removal of organic micropollutants and ammonium during managed aquifer recharge - a column study to disclose processes in reactive barriers. Water Res. 190, 116669.

NRMMC, E. and A, 2006. Australia Guidelines for Water Recycling: Managing Health and Environmental Risks (Phase 1). National Water Quality Management Strategy, Canberra.

Parkhurst, D.L., Appelo, C.A.J., 2013. PHREEQC (version 3)-a computer program for speciation, batch-reaction, one-dimensional transport, and inverse geochemical calculations. Model. Technol. B 6, 497 doi:Rep. 99-4259.

Pedretti, D., Barahona-Palomo, M., Bolster, D., Sanchez-Vila, X., Fernàndez-Garcia, D., 2012. A quick and inexpensive method to quantify spatially variable infiltration capacity for artificial recharge ponds using photographic images. J. Hydrol. 430–431, 118–126. https://doi.org/10.1016/j.jhydrol.2012.02.008.

Perujo, N., Romaní, A.M., Sanchez-Vila, X., 2019. A bilayer coarse-fine infiltration system minimizes bioclogging: the relevance of depth-dynamics. Sci. Total Environ. 669, 559–569. https://doi.org/10.1016/j.scitotenv.2019.03.126.

Porges, N., Jasewicz, L., Hoover, S., 1956. Principles of biological oxidation. Biological Treatment of Sewage and Industrial Wastes. Reinhold. Publ., New York.

Prommer, H., Barry, D.A., Chiang, W.-H., Zheng, C., 2001. PHT3D-A MODFLOW/MT3DMS-based Reactive Multi-component Transport Model.

Rittmann, B., McCarty, P., 2012. Environmental Biotechnology: Principles and Applications.

Rodríguez-Escales, P., Sanchez-Vila, X., 2016. Fate of sulfamethoxazole in groundwater: conceptualizing and modeling metabolite formation under different redox conditions. Water Res. 105, 540–550. https://doi.org/10.1016/j.watres.2016.09.034.

Rodríguez-Escales, P., Folch, A., van Breukelen, B.M., Vidal-Gavilan, G., Sanchez-Vila, X., 2016. Modeling long term enhanced in situ biodenitrification and induced heterogeneity in column experiments under different feeding strategies. J. Hydrol. 538, 127–137. https://doi.org/10.1016/j.jhydrol.2016.04.012.

Rodríguez-Escales, P., Fernàndez-Garcia, D., Drechsel, J., Folch, A., Sanchez-Vila, X., 2017. Improving degradation of emerging organic compounds by applying chaotic advection in Managed Aquifer Recharge in randomly heterogeneous porous media. Water Resour. Res. 53, 4376–4392. https://doi.org/10.1002/2016WR020333.

Rodríguez-Escales, P., Canelles, A., Sanchez-Vila, X., Folch, A., Kurtzman, D., Rossetto, R., Fernández-Escalante, E., Lobo-Ferreira, J.P., Sapiano, M., San-Sebastián, J., Schüth, C., 2018. A risk assessment methodology to evaluate the risk failure of managed aquifer recharge in the Mediterranean Basin. Hydrol. Earth Syst. Sci. 22, 3213–3227. https://doi.org/10.5194/hess-22-3213-2018.

Rubol, S., Manzoni, S., Bellin, A., Porporato, A., 2013. Modeling soil moisture and oxygen effects on soil biogeochemical cycles including dissimilatory nitrate reduction to ammonium (DNRA). Adv. Water Resour. 62, 106–124. https://doi.org/10.1016/j.advwatres.2013.09.016.

Rubol, S., Freixa, A., Carles-Brangari´, A., Ferna'ndez-Garcia, D., Romani`, A.M., Sanchez-Vila, X., 2014. Connecting bacterial colonization to physical and biochemical changes in a sand box infiltration experiment. J. Hydrol. 517, 317–327. https://doi.org/10.1016/j.jhydrol.2014.05.041.

Schaffer, M., Kröger, K.F., Nödler, K., Ayora, C., Carrera, J., Hernández, M., Licha, T., 2015. Influence of a compost layer on the attenuation of 28 selected organic micropollutants under realistic soil aquifer treatment conditions: insights from a large scale column experiment. Water Res. 74, 110–121. https://doi.org/10.1016/j.watres.2015.02.010.

Schmidt, C.M., Fisher, A.T., Racz, A., Wheat, C.G., Los Huertos, M., Lockwood, B., 2012. Rapid nutrient load reduction during infiltration of managed aquifer recharge in an agricultural groundwater basin: Pajaro Valley, California. Hydrol. Process. 26, 2235–2247. https://doi.org/10.1002/hyp.8320.

Seifert, D., Engesgaard, P., 2007. Use of tracer tests to investigate changes in flow and transport properties due to bioclogging of porous media. J. Contam. Hydrol. 93, 58–71. https://doi.org/10.1016/j.jconhyd.2007.01.014.

Silver, M., Knöller, K., Schlögl, J., Kübeck, C., Schüth, C., 2018. Nitrogen cycling and origin of ammonium during infiltration of treated wastewater for managed aquifer recharge. Appl. Geochem. 97, 71–80. https://doi.org/10.1016/j.apgeochem.2018.08.003.

Toride, N., Leij, F.J., Van Genuchten, M.T., 1995. The CXTFIT code for estimating transport parameters from laboratory or field tracer experiments. Res Rep Research R, pp. 1–138 https://doi.org/10.4016/28481.01.

Urakawa, R., Ohte, N., Shibata, H., Isobe, K., Tateno, R., Oda, T., Hishi, T., Fukushima, K., Inagaki, Y., Hirai, K., Oyanagi, N., Nakata, M., Toda, H., Kenta, T., Kuroiwa, M., Watanabe, T., Fukuzawa, K., Tokuchi, N., Ugawa, S., Enoki, T., Nakanishi, A., Saigusa, N., Yamao, Y., Kotani, A., 2016. Factors contributing to soil nitrogen mineralization and nitrification rates of forest soils in the Japanese archipelago. For. Ecol. Manag. 361, 382–396. https://doi.org/10.1016/j.foreco.2015.11.033.

Valhondo, C., Carrera, J., Ayora, C., Barbieri, M., Nödler, K., Licha, T., Huerta, M., 2014. Behavior of nine selected emerging trace organic contaminants in an artificial recharge system supplemented with a reactive barrier. Environ. Sci. Pollut. Res. 21, 11832–11843. https://doi.org/10.1007/s11356-014-2834-7.

Valhondo, C., Martínez-Landa, L., Carrera, J., Díaz-Cruz, S.M., Amalfitano, S., Levantesi, C., 2020. Six artificial recharge pilot replicates to gain insight into water quality enhancement processes. Chemosphere 240. https://doi.org/10.1016/j.chemosphere.2019.124826.

Van Der Hoek, J.P., De Fooij, H., Struker, A., 2016. Wastewater as a resource: strategies to recover resources from Amsterdam's wastewater. Resour. Conserv. Recycl. 113, 53–64. https://doi.org/10.1016/j.resconrec.2016.05.012.

WHO, 2008. Guidelines for Drinking-water Quality THIRD EDITION INCORPORATING THE FIRST AND SECOND ADDENDA Volume 1 Recommendations Geneva 2008 WHO Library Cataloguing-in-Publication Data. Guidel. Drink. Qual. 1.

Zheng, C., Wang, P., 1999. MT3DMS: A Modular Three-dimensional Multispeces Transport Model for Simulation of Advection, Dispersion, and Chemical Reactions of Contaminants in Groundwater Systems. Technical Report, Waterways Experiment Station, US Army Corps of Engineers, a Modular Three-dimensional Multi-species …